Elsevier required licence: © <2022>. This manuscript version is made available under the CC-BY-NC-ND 4.0 license http://creativecommons.org/licenses/by-nc-nd/4.0/
The definitive publisher version is available online at 10.1016/j.cej.2022.135627

CEJ-D-21-25701

# Characterization of nitrous oxide and nitrite accumulation during iron (Fe(0))- and ferrous iron (Fe(II))-driven autotrophic denitrification: mechanisms, environmental impact factors and molecular microbial characterization

Shihai Deng [a,b,*], Shuai Peng [c], Huu Hao Ngo [d], Sam Jin-An Oh [b], Zhifeng Hu [e], Hong Yao [e], Desheng Li [e,*]

[a] Institute of Global Environmental Change, School of Human Settlements and Civil Engineering, Xi'an Jiaotong University, Xi'an 710049, PR China

[b] Centre for Water Research, Department of Civil & Environmental Engineering, National University of Singapore, 1 Engineering Drive 2, Singapore 117576, Singapore

[c] State Key Laboratory of Pollution Control and Resources Reuse, College of Environmental Science & Engineering, Tongji University, Shanghai 200092, PR China

[d] Centre for Technology in Water and Wastewater, School of Civil and Environmental Engineering, University of Technology Sydney, Sydney, NSW 2007, Australia

[e] Department of Municipal and Environmental Engineering, School of Civil Engineering, Beijing Jiaotong University, Beijing 100044, PR China

* Corresponding author

S. Deng, shihai.deng@xjtu.edu.cn, (86) 15120075057

D. Li, dsli@bjtu.edu.cn, (86) 13371116611

**Abstract**

The iron (Fe(0))-/ferrous iron (Fe(II))-driven autotrophic denitrification (ADN) have been alternative methods for nitrogen removal from low organic carbon (OC) wastewater, but the accumulation of nitrous oxide ($N_2O$) and nitrite ($NO_2^-$) along with these processes remains unclear. This research aimed to systematically characterize the $N_2O$/$NO_2^-$ accumulation in Fe(0)-/Fe(II)-ADN processes through investigating the mechanisms, impact factors, and molecular biological characteristics. Results showed that Fe(II)-ADN was effective in $NO_3^-$ reduction but was less efficient in $N_2O$ reduction ($k$ = 0.50 $h^{-1}$) than Fe(0)-ADN ($k$ = 1.82 $h^{-1}$). $NO_2^-$/$N_2O$ accumulation in Fe(II)-ADN (28.6%/30.7%) was much higher than Fe(0)-ADN (12.6%/1.5%). Introducing hydrogenotrophic denitrification (H-ADN) into Fe(II)-ADN system significantly ($p < 0.05$) reduced $NO_2^-$/$N_2O$ accumulation. Fe(0)-ADN was proved a coupled process of Fe(II)- and H-ADN by *in-situ* generating Fe(II)/$H_2$, and Fe(II)-ADN and H-ADN mainly contributed to $NO_3^-$ and $NO_2^-$/$N_2O$ reduction, respectively. Optimum pH (7.5) and temperature (30-35 °C) were confirmed with controlled $NO_2^-$/$N_2O$ accumulation and effective denitrification. Dosing inorganic carbon (IC) and OC enhanced denitrification and reduced $NO_2^-$/$N_2O$ accumulation, where OC was more efficient with an optimum dosage of 0.25 mmol C/mmol N. 16S rRNA high-throughput sequencing and *Pearson* Correlation Coefficients verified that *Thiobacillus* was the main contributor to $NO_3^-$ reduction, whereas *Thauera* and *Acidovorax* possessed high $NO_2^-$/$N_2O$ reduction capability. Real-time quantitative polymerase chain reaction and enzyme activity assay demonstrated that the nitrite reductase encoded by gene *nirK* and the nitrous oxide reductase encoded by gene *nosZ* were efficient in catalyzing the further reduction of $NO_2^-$ and $N_2O$, respectively. This study could provide an in-depth understanding of $NO_2^-$/$N_2O$ accumulation in Fe(II)-/Fe(0)-ADN processes and contribute to their application,

optimization and secondary pollutants control.

**Keywords**

Zero-valent iron (Fe(0)); ferrous iron (Fe(II)); autotrophic denitrification; nitrate ($NO_3^-$); nitrite ($NO_2^-$); nitrous oxide ($N_2O$)

## 1 Introduction

Nitrate ($NO_3^-$) has been identified as one of the most critical pollutants in surface water and groundwater [1, 2]. The contamination of $NO_3^-$ in these water resources has markedly increased the incidence rates of human diseases, including the methemoglobinemia and non-Hodgkin's lymphoma [3]. Both the World Health Organization (WHO) [4] and the United States Environmental Protection Agency (USEPA) [5] have set a maximum $NO_3^-$ contaminant level of 10 mg N/L in surface water. The advanced denitrification has remained difficult as both surface water and groundwater contain a low concentration of organic carbon (OC), which could hardly sustain heterotrophic denitrification (HDN) [6, 7]. Obtaining the advantages of utilizing inorganic carbons (IC, i.e., $CO_3^{2-}$ and $HCO_3^-$) as carbon sources and inorganic reductants (e.g., hydrogen ($H_2$) and sulfur compounds ($S^0/S^{2-}/S_2O_3^{2-}$)) as electron donors, autotrophic denitrification (ADN) is receiving increasing interest in low-organic-carbon water treatment [6, 8].

Alternatively, iron-compounds-supported ADN processes (Fe-ADN), including ferrous iron-driven ADN (Fe(II)-ADN) and zero-valent iron-driven ADN (Fe(0)-ADN), have attracted grown attention in the past decade [9-12]. Fe-ADN possesses the advantage of the widely accessible iron sources, including the iron scraps from the metal processing factory and the iron ore resource [13, 14]. The adoption of Fe-ADN could also avoid the safety risk of H-ADN process [3, 6] and the secondary pollution of $SO_4^{2-}$ in the sulfur compounds-driven ADN processes (S-ADN) [6, 15]. The proposed reaction mechanism

of Fe(II)-ADN is shown as Eq. (1) [10, 12]. The Fe(0)-ADN process could be initiated by the *in-situ* generation of Fe(II) and hydrogen ([H]/$H_2$) through Fe(0)-corrosion in water (Eq. (2)), and subsequently proceed Fe(II)-ADN and hydrogenotrophic denitrification (H-ADN, Eq. (3)) [12, 16].

$$5.48\ Fe^{2+} + NO_3^- + 0.12\ CO_2 + 0.024\ NH_4^+ + 3.264\ H_2O \rightarrow 5.48\ Fe^{3+} + 6.456\ OH^- + 0.50\ N_2 + 0.024\ C_5H_7O_2N \quad (1)$$

$$Fe(0) + 2H_2O \rightarrow Fe^{2+} + 2[H]\ (\text{or}\ H_2) + 2OH^- \quad (2)$$

$$0.99\ H_2 + 0.05\ CO_2 + 0.35\ H^+ + 0.35\ NO_3^- \rightarrow 0.01\ C_5H_7O_2N + 1.13\ H_2O + 0.17\ N_2 \quad (3)$$

Nitrous oxide ($N_2O$) is a potent greenhouse gas that possesses 296-fold the warming effect of carbon dioxide [17, 18]. It has also been reported to be toxic to the human body by inactivating Vitamin $B_{12}$ [19]. Denitrification in wastewater treatment plants (WWTP) has been recognized as an anthropogenic $N_2O$ source [20-22]. WWTP is recognized as a considerable hotspot of the accumulation of nitrite ($NO_2^-$), which has performed direct hazardous effects on both human beings and animals [23, 24]. As Rocher et al. (2015) tested in a full-scale plant (240,000 $m^3$/day) located in Paris, the effluent $NO_2^-$ could reach 10% of the removed $NO_3^-$ when the carbon source was not properly supplied [25]. Zhou et al. (2011) demonstrated that $NO_2^-$ is known to accumulate in WWTPs under certain environmental conditions, especially when pH was below 6.8 [26]. Liu et al. (2016) successfully set up a mathematical model based on the activated sludge model (ASM) to describe the $N_2O$ accumulation in the sulfide-based AD process, which demonstrated that a substantial amount of $N_2O$ could accumulate during the initial stage due to the relatively low autotrophic $N_2O$ reduction rate [27]. Generally, the biological denitrification process involves four steps with the stepwise reduction of $NO_3^-$ through $NO_2^-$, nitric oxide (NO) and $N_2O$ into nitrogen gas ($N_2$) under the catalysis of the periplasmic/membrane nitrate reductases (NAP/NAR, encoded by gene *napA*), nitrite reductase (NIR, encoded by genes

*nirK* and *nirS*) and nitric oxide reductase (NOR, encoded by gene *norB*) and nitrous oxide reductase (NosZ, encoded by gene *nosZ*), respectively [28-30]. Although existing studies have characterized the accumulation of $N_2O$ and $NO_2^-$ in H-ADN [31] and S-ADN [27, 32] processes, a relevant survey on the Fe(II)- and Fe(0)-ADN processes can be rarely found, let alone a systematical study on the accumulating mechanisms, impact factors and molecular biological characteristics.

Increasing evidence has demonstrated the accumulation of $NO_2^-$ and $N_2O$ in Fe(II)- [9, 33] and Fe(0)-ADN [12] processes, particularly the accumulation of $N_2O$. In the Fe(II)-ADN process, a $N_2O$ accumulation of over 60% of initial nitrogen had been confirmed [9]. Meanwhile, $N_2O$ accumulation percentage of 9.2% has been observed in the Fe(0)-ADN process [12]. These $N_2O$ accumulation percentages are much higher than that in the H-ADN ($\leq 0.75\%$) [31] and S-ADN ($\leq 0.41\%$) [32, 34] processes. Nevertheless, no proper strategies have been raised to control the accumulation due to lack of understanding of the mechanisms and impact factors.

Existing studies have verified that environmental factors, such as pH, temperature and carbon source supply, can affect denitrification by affecting the microbial activity and $NO_x$ reduction rates [27, 31]. Moreover, Fe(0)-ADN could proceed through the *in-situ* generation of Fe(II) and $H_2$. It was proved that the composition of electron donors could also affect $NO_x$ reduction by changing microbial composition, gene abundance and enzyme activity [12, 31, 35]. However, the roles of Fe(II) and $H_2$ in the accumulation of $NO_2^-$ and $N_2O$ in Fe(0)-ADN remains unclear. Therefore, a comprehensive study is essential to unveil the $NO_x$ reduction kinetics, microbial community compositions, functional genes and critical enzymes of Fe(II)/Fe(0)-ADN, and evaluate the factors affecting $N_2O$ and $NO_2^-$ accumulation.

In this study, Fe(II)-, Fe(0)- and H-ADN reactors were set up and operated under

various conditions to characterize the $N_2O$ and $NO_2^-$ accumulation. The aims are to 1) characterize the $NO_3^-$, $NO_2^-$ and $N_2O$ reduction of Fe(II)- and Fe(0)-ADN processes; 2) explore the roles of Fe(II)- and H-ADN in nitrogen removal and accumulation of $NO_2^-$ and $N_2O$ in Fe(0)-ADN process; 3) investigate the dominant microbes, functional genes and key enzymes related to $NO_2^-$ and $N_2O$ accumulation in denitrifying cultures. 4) evaluate the effects of pH, temperature and carbon source supply on $NO_2^-$ and $N_2O$ accumulation. This study will provide a comprehensive and in-depth understanding of $N_2O$ and $NO_2^-$ accumulation in Fe(II)-/Fe(0)-ADN processes, which will contribute to their application and optimization.

## 2 Material and methods

### 2.1 Chemical reagents, materials and compressed gases

$FeCl_2 \cdot 4H_2O$ (analytical reagent, AR) was utilized as Fe(II) source for Fe(II)-ADN. $KNO_3$ (AR) and $NaNO_2$ (AR) synthesized initial nitrogen in the tests. $NaHCO_3$ (AR) and $CH_3COONa$ (AR) synthesized IC and OC, respectively. NaOH (AR) and HCl (12 M) were used to prepare alkaline and acidic stock solutions for pH adjusting. The $NaH_2PO_4 \cdot 2H_2O$ (AR), KI (AR), $H_3BO_3$ (AR), $MgSO_4 \cdot 7H_2O$ (AR), $ZnSO_4 \cdot 7H_2O$ (AR), $CaCl_2 \cdot 2H_2O$ (AR), $CuSO_4 \cdot 5H_2O$ (AR), $CoCl_2 \cdot 6H_2O$ (AR) and $Na_2MoO_4 \cdot H2O$ (AR) were used to prepare microelement stock solution to support microorganism growth [12]. All the chemical reagents were purchased from Sinopharm Chemical Reagent Ltd, China. ZVI particles (≥ 99.5%, 25-50 μm, Taixinglong Metal Fitting Factory Ltd, China) and granular activated carbon (GAC, BET ≥ 800 $m^2/g$, 50-100 μm, Green Source Ltd, China) were used to form Fe(0)-carbon galvanic-cells (Fe(0)/C) to initiated Fe(0)-ADN process. Compressed $H_2$ (≥ 99.99%, 4N) was used to support the H-ADN process, and compressed $N_2$ (4N) was adopted to dilute $H_2$ to control the $H_2$-dosage. Compressed $N_2O$ (≥ 98%) was used for the $N_2O$ reduction experiment. All the compressed gases were purchased

from Ling-Gas Ltd, China. Milli-Q water (≥ 18 Ω) was used in synthetic wastewater preparation and sample test.

**2.2 Set-up of the Fe(0)-, Fe(II)- and H-ADN reactors**

Nine sealable serum bottles (1000-mL version, Schott-Duran®, Germany) with a capacity of 1100 mL were used to set up reactors. All batch tests were carried out in the constant temperature shaker (HT-2102S, HerryTech®, China). In all batch tests, the reactors' working volume (volume of mixed liquor) was controlled at 500 mL, maintaining a 600-mL headspace. All the reactors were inflated by $N_2$ before operation. The weighted $FeCl_2 \cdot 4H_2O$ was directly dosed into the mixed liquor in the reactors to initiate Fe(II)-ADN. In H-ADN tests, the mixture of $H_2$ and $N_2$ with required $H_2$ concentrations was first inflated into serum bottle using the vacuum dewatering method; then, 500 mL of mixed liquor of raw wastewater and biomass was injected into the bottle and 500 mL of the gas mixture was expelled at the same time.

In Fe(0)-ADN tests, the direct supply of ZVI particles usually results in fast passivation on the particle surface [36, 37]. Therefore, a media which was developed based on Fe(0)/C galvanic-cells was adopted [12, 38]. With the formation of Fe(0)/C galvanic-cells [12, 39], the oxidation reaction on ZVI-anode (Eq. 4) and the reduction reaction on C-cathode (Eq. 5) could proceed separately to avoid the passivation of ZVI during corrosion (Eq. 1). The ZVI particles and GAC were used as active compounds in the Fe(0)/C media at a mass ratio of 8:1 with a volume ratio of approximately 1:1 for the effective contact of ZVI particles and GAC in water, thereby effectively forming Fe(0)/C galvanic-cells [12, 38]. Fig. S1 (shown in supplementary information) showed the preparation process of the media. In the experiments, 100 mL (252 ± 22 g, containing about 202 g Fe(0)) media was dosed in the reactor to initiate Fe(0)-ADN process. As tested, the Fe(0)/C media obtained a Fe(II) and $H_2$ production of more than 0.8 mM/h

(Fig. S2).

ZVI-anode: $Fe \rightarrow Fe^{2+} + 2e^{-}$, $\varphi^{0}(Fe/Fe^{2+}) = 0.44$ V (4)

C-cathode: $2H^{+} + 2e^{-} \rightarrow H_2/2[H]$, $\varphi^{0}([H]/H^{+}) = 0.00$ V (5)

**2.3 Acclimation and cultivation of denitrifying cultures**

The initial inoculum was collected from the secondary settling tank of a local WWTP in Singapore. A concentrated denitrifying culture of the initial inoculum with a mixed liquor suspended solids (MLSS) of 6.7 ± 0.2 g/L was prepared. 100-mL concentrated denitrifying culture was inoculated into the 500-mL liquid phase of reactors. Before batch tests were initiated, the denitrifying systems were trained by periodically (every 24 hours) feeding with the corresponding electron donor and synthetic wastewater containing $NO_3^-$ (40 mg N/L) and microelements ($NaH_2PO_4 \cdot 2H_2O$, 5.0 mg/L; KI, 0.18 mg/L; $H_3BO_3$, 0.15 mg/L; $MgSO_4 \cdot 7H_2O$, 1.9 mg/L; $CaCl_2 \cdot 2H_2O$, 8.18 mg/L; $ZnSO_4 \cdot 7H_2O$, 0.12 mg/L; $CuSO_4 \cdot 5H_2O$, 0.03 mg/L; $CoCl_2 \cdot 6H_2O$, 1.61 mg/L; and $Na_2MoO_4 \cdot H_2O$, 0.06 mg/L) [40]. The steady-state of the denitrifying cultures was confirmed after the denitrification performance remained constant. After cultivation, the sludge in the reactors was condensed or diluted to control a volatile suspended solids (VSS) level of 2.5 ± 0.1 g/L.

**2.4 Experimental study**

In this study, three batch-test groups were designed (as shown in Table 1), among which, batch-test group A was targeted to characterize the reductive reactions of $NO_3^-$, $NO_2^-$ and $N_2O$ in the ADN systems, batch-test group B was designed to investigate the contributions of Fe(II)- and $H_2$ to $NO_2^-$ and $N_2O$ accumulations, and batch-test group C was conducted to evaluate the environmental factors affecting the $NO_2^-$ and $N_2O$ accumulations.

In group A, the Fe(0)- and Fe(II)-ADN are characterized by utilizing $NO_3^-$, $NO_2^-$ and $N_2O$ as sole electron-donors. In the $NO_3^-$ and $NO_2^-$ reduction experiments, an initial

concentration of 40 mg ($NO_3^-$ or $NO_2^-$)-N/L was provided, which is in the range of nitrogen concentration (30-50 mg N/L) in contaminated groundwater [27, 41]. In the $N_2O$ reduction tests, the purchased $N_2O$ was injected to maintain an equivalent initial concentration of 40 mg $N_2O$-N/L after normalizing to the mixed liquor volume. In Fe(II)-ADN tests, Fe(II) was dosed at 7.6 mmol/mmol N, which was equal to the electron supplied by Fe(0)/C in Fe(0)-ADN tests within 12-h (Text S1 and Fig. S1 in the supplementary information). The pseudo-first-order kinetics ($-\ln(C_t/C_0) = k_1 t$) and pseudo-zero-order kinetics ($-(C_t - C_0) = k_2 t$) were applied to evaluate the $NO_3^-$, $NO_2^-$ and $N_2O$ reduction rates (Text S2). The residual sum of squares (RSSQ) was calculated through Eq. S3 to evaluate the approximation of $NO_3^-$, $NO_2^-$ and $N_2O$ reduction process in Fe(0)-/Fe(II)-ADN to the pseudo-first-kinetic and pseudo-zero-kinetic equations (Text S2). Batch-test group B was carried out using $NO_3^-$ as the sole electron acceptor, and Fe(II) and $H_2$ were supplied as electron donors at different compositions (mmol Fe(II):mmol $H_2$) of 8:0, 16:0, 12:2, 8:4, 4:6, 0:8 and 0:4. In batch-test group C, the impacts of pH, temperature, IC and OC on $NO_2^-$ and $N_2O$ accumulation were investigated in the ranges of 6-8.5, 10-45 °C, 0-1 mmol C/mmol N and 0-1 mmol C/mmol N, respectively, according to the previous studies [12, 31].

**2.5 Sampling and analytical methods**

Before testing, water samples were taken in triplicate by a syringe and subsequently filtered through the Millipore filters (0.45 μm). Analytical methods suggested by the Standard Methods for the Examination of Water and Wastewater（21th ed, APHA) were applied for the analysis of $NO_3^-$-N (4500-$NO_3^-$), $NO_2^-$-N (4500-$NO_2^-$), $Fe^{2+}$ (3500-Fe), MLSS (2540B), and VSS (2540E) (APHA, 2005). A spectrophotometer (UV-1800PC, MAPADA®, China) was used for UV-VIS spectrometry analysis, and a pH meter (S220-K, Mettler-Toledo®, USA) was used in pH adjusting.

Samples of the headspace gas were collected using gasbags for $N_2O$ and $H_2$ detection. $N_2O$ (g) in the headspace was analyzed by gas chromatography (GC) (Agilent 6890N, USA) with a Porapak-Q packing column and an electron capture detector. $H_2$ (g) was measured by GC (Agilent 6890, USA) with a Carbonxen-1000 packing column and a thermal conductivity detector. The detailed chromatographic conditions have been provided in Text S3. Henry's law ($C_{aq} = HE \cdot P_g$; $P_g = X_g \cdot atm$) was applied to calculate the dissolved $N_2O$ (aq) and $H_2$ (aq) in aqueous phase (Text S4) [42]. In the evaluation of $N_2O$ accumulation under different temperatures, Henry's law constant (*HE*) of $N_2O$ varies with temperature as *HE* ($N_2O$) = $1.17 \times 10^{-7}$ exp(2284/*T*) [43] (Text S4). Finally, units of the detected $N_2O$ and $H_2$ were normalized to milligram per liter reaction volume, and the sums of $N_2O$ (g) & $N_2O$ (aq) and $H_2$ (g) & $H_2$ (aq) respectively represent the total $N_2O$ and $H_2$ concentrations.

**2.6 Molecular microbial analysis**

*2.6.1 DNA Extraction, PCR amplification and 16S rRNA high-throughput sequencing*

Samples of the inoculation activated sludge (IAS) and the trained denitrifying cultures of Fe(II)-, Fe(0)- and H-ADN systems (namely BioFe(II), BioFe(0) and BioH, respectively) were taken in triplicate. The samples from the same system were mixed and centrifuged at 5,000 rpm under 4 °C for 10 min. Genomic deoxyribonucleic acid (DNA) was subsequently extracted in triplicate from the deposit with DNA Isolation Kits (E.Z.N.A.®, USA) for further analysis. The universal primer pare 338F (5'-ACTCCTACGGGAGGCAGCAG-3')/806R (5'-GGACTACHVGGGTWTCTAAT-3') was utilized for polymerase chain reaction (PCR) amplification at 16S rRNA gene level. High-throughput sequencing (HTS) was performed on the obtained products using the Illumina® MiSeq platform. After quality filtration, 35,073, 39,438 and 33,635 valid sequences were obtained from the samples, respectively. Operational taxonomic units

(OTUs) were clustered with the UPARSE platform (Version7.0) under a similarity threshold of ≥ 97%, and a totally 1274 OTUs were obtained. Principal component analysis (PCA) was performed among the samples with *R*-code. The I-Sanger Cloud platform (Majorbio®, Shanghai, China) was used for microbial distribution analysis.

*2.6.2 Real-time qPCR and enzymatic activity assay*

In this study, enzymes that determine the reduction rates of $NO_3^-$, $NO_2^-$ and $N_2O$ were analyzed, including the NAP and NAR catalyzing $NO_3^-$ reduction, the NIR catalyzing $NO_2^-$ reduction and the NosZ catalyzing $N_2O$ reduction. The genes *napA* (encodes NAP and NAR), *nirS* and *nirK* (both encode NIR), and *nosZ* (encodes NosZ) were also detected to evaluate their relationship with $NO_2^-$ and $N_2O$ accumulation. The DNA extraction products obtained in section *2.6.1* were also used for gene quantification with real-time quantitative polymerase chain reaction (qPCR). The primers, thermal cycles, mixtures compositions and detailed analysis processes applied in qPCR for each targeted gene were described in Text S5. All the enzymatic activities were based on the protein content that was measured with bovine serum albumin as a standard [29, 44]. The detailed methods for the enzyme activity assay are provided in Text S6. The activity of enzymes and quantity of genes detected from the sample IAS were set to 100%, and that from the BioFe(II), BioFe(0) and BioH samples were presented as relative enzyme activities and relative gene quantities on the basis of the sample IAS.

**2.7 Statistical analysis**

All the samples were tested in triplicate, and the mean value and standard deviation were calculated. The *Pearson* correlation coefficient (PCC) was performed to evaluate the correlation, in which PCC at (–0.4, 0.4), (–0.7, –0.4] & [0.4, 0.7) and (–1, –0.7] & [0.7, 1) were identified as uncorrelated, correlated and highly correlated, respectively. The positive value and negative value of PCC were identified as positively and negatively

correlated, respectively. Analysis of variance (ANOVA) was conducted to test the significance, where $p(0.05) < 0.05$ was identified as statistically significant.

## 3. Results and discussion

### 3.1 $NO_3^-$, $NO_2^-$ and $N_2O$ reduction characteristics in Fe(0)-/Fe(II)-ADN

Fe(0)-ADN and Fe(II)-ADN were characterized utilizing $NO_3^-$, $NO_2^-$ and $N_2O$ as the sole electron acceptors. The $NO_3^-$, $NO_2^-$ and $N_2O$ in all tests have been depleted within a reaction duration of 10.5 h. As Fig. 1 shows, Fe(II)-ADN performed a faster $NO_3^-$ depletion but a weaker $N_2O$ reduction. When pseudo-first-order kinetics was applied (Table 2), Fe(II)-ADN obtained $NO_3^-$, $NO_2^-$ and $N_2O$ reduction rate constants ($k_1$) of 1.7, 3.8 and 0.5 $h^{-1}$, while that were 1.2, 1.8 and 1.9 $h^{-1}$ for Fe(0)-ADN, respectively, demonstrating that Fe(II)-ADN was more efficient in $NO_3^-$/$NO_2^-$ reduction but much less efficient in $N_2O$ than Fe(0)-ADN. The specific $NO_3^-$, $NO_2^-$ and $N_2O$ reduction rates ($K$) of 0.9, 1.6, and 0.3 kg N/(kg VSS·d) were calculated for Fe(II)-ADN, and that of 0.5, 1.5 and 1.6 kg N/(kg VSS·d) were calculated for Fe(0)-ADN, respectively. According to the research of Li et al. (2017), H-ADN process could achieve a $K(N_2O)$ of 3.96 kg N/(kg VSS·d), which is much higher than the Fe(0)- and Fe(II)-ADN processes in this study. It could be speculated that H-ADN might be the main contributor to $N_2O$ reduction in Fe(0)-ADN process. Furthermore, the results of kinetic analysis (Table 2) showed that the $NO_3^-$ and $NO_2^-$ reduction in Fe(II)-ADN was better fitted to the pseudo-zero-order kinetics (with RSSQ of 161.5 and 149.0, respectively) than the pseudo-first-order kinetics (with RSSQ of 409.0 and 294.8, respectively). While, the $N_2O$ reduction in Fe(II)-ADN was better fitted to pseudo-first-order kinetics obtaining RSSQ of 34.4, which was much lower than the 769.0 obtained from the pseudo-zero-order kinetics. Comparatively, all of the $NO_3^-$, $NO_2^-$ and $N_2O$ reduction processes in Fe(0)-ADN were better fitted to pseudo-first-order kinetics with much lower RSSQ than the pseudo-zero-order kinetics. The results

demonstrated that the $NO_3^-$ and $NO_2^-$ reduction in Fe(II)-ADN was close to the zero-order chemical reaction process, while that of the Fe(0)-ADN was more consistent with the pseudo-first-order bioprocess. Moreover, $N_2O$ reduction in both processes can be well explained as a pseudo-first-order bioprocess.

Noteworthy, Fe(II)-ADN process showed a much higher $NO_2^-$ and $N_2O$ accumulation in the $NO_3^-$ reduction test, with a maximum $NO_2^-$ accumulation percentage of 28.6% and a maximum $N_2O$ accumulation percentage of 31.9%. While that was only 12.8% and 1.5% in Fe(0)-ADN process, respectively. As Li et al. (2017) demonstrated, the maximum $N_2O$ accumulation in H-ADN could be as low as 0.04% and 0.75% during $NO_3^-$ and $NO_2^-$ reduction, respectively. The results suggest that Fe(0)-ADN possesses a much higher $N_2O$ reduction capacity than Fe(II)-ADN process due to the presence of H-ADN, which might be the main contributor to the $N_2O$ reduction.

**3.2 Contributions of Fe(II)- and H-ADN processes in Fe(0)-ADN system**

Fe(II) and $H_2$ were supplied as electron-donors at different compositions (mmol Fe(II):mmol $H_2$) to evaluate the impact of Fe(II) (at 8:0 and 16:0), $H_2$ (at 0:8 and 0:4) and Fe(II)/$H_2$ ratio (16:0, 12:2, 8:4, 4:6 and 0:8). As shown in Fig. 2, the increase of Fe(II) dosage from 8 to 16 mmol and the increase of $H_2$ dosage from 4 to 8 mmol both markedly enhanced the denitrification process. Comparatively, Fe(II)-ADN at Fe(II) dosage of 16 mol showed faster $NO_3^-$ reduction than H-ADN at $H_2$ dosage of 8 mmol. It is noteworthy that high $NO_2^-$ and $N_2O$ accumulation was observed in Fe(II)-ADN (at 16:0) with accumulation percentages of 24.0% and 25.3%, respectively (Fig. 2(d)). However, in the H-ADN process, even insufficient $H_2$ (4 mmol) was supplied, a low $N_2O$ accumulation percentage of 0.31% was observed, which further decreased to 0.18% when at $H_2$ dosage of 8 mmol. This result is in accordance with the literature that the $N_2O$ accumulation percentage in H-ADN process was below 0.75%) [31]. It was significantly ($p < 0.05$)

lower than Fe(II)-ADN system. This result confirmed the research of Lu et al. (2009) that the reductase NosZ was more competitive in $H_2$ utilization than reductase NIR, and no massive $N_2O$ accumulation was observed even when a low $H_2$ dosage of 0.03 mg/L was applied ($R^2 > 0.96$).

The presence of H-ADN in Fe(II)-ADN process at Fe(II)/$H_2$ ratio of 12:2 markedly reduced $N_2O$ accumulation from 25.3% to 5.5% (Fig. 2(c)). It further decreased to 1.1% and 0.8% when changing Fe(II)/$H_2$ ratio to 8:4 and 4:6, respectively, which were significantly ($p < 0.05$) lower than Fe(II)-ADN (16:0). A gradual drop in $NO_3^-$ reduction rate was observed, obtaining $K(NO_3^-)$ of 0.80, 0.57, 0.55, and 0.41 kg N/(kg VSS·d) at Fe(II)/$H_2$ ratio of 16:0, 12:2, 8:4 and 4:6, respectively. These results demonstrated that Fe(II)-ADN was efficient in $NO_3^-$ reduction producing $NO_2^-$ and $N_2O$, and the further reduction of $NO_2^-$ and $N_2O$ by H-ADN effectively controlled the accumulation of $NO_2^-$ and $N_2O$. It also suggested that introducing H-ADN into the Fe(II)-ADN system could be an effective strategy for controlling $NO_2^-$ and $N_2O$ emissions during denitrification. Correspondingly, introducing Fe(II)-ADN into the H-ADN system could effectively enhance the denitrification process. In this study, the optimum Fe(II)/$H_2$ ratio of 8:4 was confirmed.

### 3.3 Environmental factors affecting $NO_2^-$ and $N_2O$ accumulation of Fe(0)-ADN

#### *3.3.1 The influence of pH*

The denitrification and accumulation of $NO_2^-$ and $N_2O$ were characterized through gradually increasing pH from 6 to 8.5. As Fig. 3 shows, the decrease of pH value continuously enhanced the reduction of $NO_3^-$ in Fe(0)-ADN process. $K(NO_3^-)$ of 0.86, 0.57, 0.43, 0.41, 0.36 and 0.20 kg N/(kg VSS·d) were obtained at pH of 6, 6.5, 7, 7.5, 8 and 8.5, respectively (Fig. 4(a)). As has been concluded that the $NO_3^-$ was mainly reduced by Fe(II)-ADN in Fe(0)-ADN process, Fe(II) generation rate from Fe(0)-corrosion was

the key impact factor of $NO_3^-$ reduction. A lower pH could significantly benefit the Fe(II) and $H_2$ production from Fe(0) [45]. However, an immense $NO_2^-$ and $N_2O$ accumulation was found at pH of 6 and 6.5 (Fig. 3), which demonstrated the weak $NO_2^-$ and $N_2O$ reduction at low pH. Whereas their accumulation significantly dropped when pH was increased over 7. Maximum $NO_2^-$ and $N_2O$ accumulation percentages remained at the ranges of 3.6%-4.1% and 0.42%-0.52% at pH of 7.5-8.5, respectively. The results indicated that enzyme NIR and NosZ could remain high activity under the slightly alkaline conditions but were inhibited under acidic conditions. A sharp decrease in $NO_2^-$ and $N_2O$ accumulation has also been observed in HDN [46] and H-ADN processes [31] when increasing pH above 7. Chen et al. (2020) demonstrated that NIR and NosZ could be inhibited by the free nitrous acids (FNA). As nitrous acid is a weak electrolyte, FNA could be easily formed under acidic conditions [47]. As Zhou et al. (2008) reported, the inhibition of FNA on NosZ was more severely (even when FNA was as below as $0.7\times10^{-3}$ mg N/L) than that on NIR, causing proton motive force collapse by increasing proton permeability through the cell membranes, inhibiting the synthesis of adenosine triphosphate (ATP). Moreover, FNA could be more easily combined with the active sites of NosZ than $N_2O$ leading to an inhibited $N_2O$ reduction [26, 31].

Noteworthy, Fe(0)-ADN process obtained a higher $N_2O$ accumulation (1.9%) at neutral condition (pH = 7), comparing to the HDN process (< 0.2%) [46] and the H-ADN process (< 0.1%) [31]. When adjusting pH to 7.5, the accumulation percentages of $NO_2^-$ (4.1%) and $N_2O$ (0.51%) both dropped. Although a slightly lower $NO_2^-$ and $N_2O$ accumulation was achieved at high pH of 8-8.5, the $K(NO_3^-)$ dropped due to the inhibition of alkaline environment on Fe(0)-corrosion (Fig. 4(a)). Consequently, 7.5 was selected as the optimum pH for Fe(0)-ADN considering both denitrification rate and the accumulation of $NO_2^-$ and $N_2O$, which was higher than that in the H-ADN process

obtained by Li et al. (2017).

*3.3.2 The influence of temperature*

Studies have described the positive correlation between denitrification rate and temperature at the range of 10-30 °C in HAD processes [48, 49]. While in the H-ADN process, Li et al. (2017) obtained an optimum temperature of 40 °C, considering both the denitrification rate and the accumulation of $NO_2^-$ and $N_2O$. Hence, the optimum temperature would be different with different electron donor types, and the accumulation of $NO_2^-$ and $N_2O$ should also be considered in optimizing temperature. The present study investigated the performance and $NO_2^-$/$N_2O$ accumulation of Fe(0)-ADN at a temperature range of 10-45 °C. As Fig. 3(b1) shows, at the temperature range of 10-40 °C, the reduction of $NO_3^-$ was enhanced with the increase of temperature. The $K(NO_3^-)$ of Fe(0)-ADN gradually increased from 0.24 to 0.67 kg N/(kg VSS·d), and a relatively high $K(NO_3^-)$ was obtained at the temperature range of 30-40 °C (Fig. 4(b)). The decrease of $NO_2^-$ accumulation was also observed at the temperature range of 10-40 °C (Fig. 3(b2)). The results demonstrated that the increase of temperature from 10 to 40 °C could enhance the $NO_3^-$ and $NO_2^-$ reduction. While, when the temperature was continuously increased to 45 °C, a decrease of $K(NO_3^-)$ and an increase of $NO_2^-$ accumulation were observed, demonstrating that the exorbitant temperature could inactivate the enzymes NAP, NAR and NIR. This study confirmed a suitable temperature range of 30-40 °C for $NO_3^-$ and $NO_2^-$ reduction in Fe(0)-ADN.

Fig. 3(b3) and Fig. 4(b) show the variation of $N_2O$ accumulation in Fe(0)-ADN with temperature. At the temperature range of 10-30 °C, $N_2O$ accumulation gradually decreased from 3.9% to 0.35%, and a plummet decrease was observed when increasing temperature from 20 °C to 25 °C. The result showed that the suitable temperature of reductase NosZ in the Fe(0)-ADN process should be ≥ 25 °C, higher than that for NIR

[31]. However, $N_2O$ accumulation slightly increased to 0.76% at 35 °C. With the continuous increase of temperature to 40 °C and 45 °C, a remarkable rise of $N_2O$ accumulation to 3.0% and 7.4% was observed, respectively (Fig. 4(b)). Hence, a suitable temperature range of 25-35 °C was confirmed for $N_2O$ control of Fe(0)-ADN process. Except for the inhibition of high temperature on NosZ, other vital factors that inhibit the $N_2O$ reduction are the reduced solubility of $N_2O$ and the increased FNA formation at high temperature [26, 50]. Consequently, an optimal temperature range of 30-35 °C was suggested for the Fe(0)-ADN process.

### 3.4 Control of $NO_2^-$ and $N_2O$ accumulations by dosing IC and OC

Though studies have demonstrated the impacts of carbon source supply on the HDN, H-ADN, and S-ADN processes [31, 46, 51], the Fe(0)-ADN process has not been comprehensively described. Fig. 5 and Fig. 6 show the effects of IC and OC dosages on denitrification and the accumulation of $NO_2^-$ and $N_2O$ in Fe(0)-ADN process. At IC to nitrogen ratio of 0, 0.25, 0.5 and 1 mmol C/mol N, $K(NO_3^-)$ of 0.22, 0.29, 0.35 and 0.36 kg N/(kg VSS·d) were respectively obtained, while that were 0.22, 0.54, 0.58 and 0.66 kg N/(kg VSS·d) at the same dosage of OC. The results showed that denitrification was not terminated when no carbon source was added (Fig. 5(a1) and (b1)), which confirmed the explanation that the dissolution of microbial cells could support the denitrifying process [6]. As Fig. 5 shows, adding carbon sources significantly enhanced the denitrification process. The optimal IC dosage of 0.5 mmol C/mmol N could be confirmed for Fe(0)-ADN. Li et al. (2017) also showed the enhancement of IC on H-ADN process but obtained a lower optimal IC dosage of 0.18 mmol C/mmol N. Comparatively, OC obtained a much higher $K(NO_3^-)$ increment than IC. It confirmed the existing studies that OC could be better utilized by the assimilation process of microorganisms than IC [6, 12]. With the continuous increase of OC dosage to 1 mmol C/mmol N, $K(NO_3^-)$ jumped to

0.66 kg N/(kg VSS·d), indicating that the HDN process utilizing OC as electron donor started to dominate the denitrification process. Deng et al. (2020) also demonstrated that the HDN started to dominate the Fe(0)-ADN process when the initial chemical oxygen demand to $NO_3^-$-N ratio was over 1.5 (i.e., 0.56 mmol C/mmol N). Consequently, the optimal IC dosage of 0.5 mmol C/mmol N and the optimal OC dosage of 0.25 mmol C/mmol N were confirmed for denitrification enhancement, respectively.

As shown in Fig. 5(a2)-(a3) and (b2)-(b3), the dose of IC and OC both reduced the accumulation of $NO_2^-$ and $N_2O$. IC dosage of 0.25 mmol C/mmol N reduced the $NO_2^-$ and $N_2O$ accumulation. When IC dosage was increased to 0.5-1 mmol C/mmol N, the $N_2O$ accumulation percentages decreased and remained relatively stable at 1.3-1.6% (Fig. 6(a)). However, no pronounced reduction in the $N_2O$ accumulation was observed in the OC dosage was further increased to 0.5-1 mmol C/mmol N, and the $N_2O$ accumulation remained stable at 0.15%-0.21% (Fig. 6(b)). It could be concluded that OC was more efficient than IC in the control of $NO_2^-$/$N_2O$ accumulation. The mechanism could be explained by Eq. (6)-(8), showing an easier activation of hybrid respiration on the reductases by OC [6, 12].

$$2H\text{—}R + UQ \xrightarrow{DeH} 2R + UQH_2 \quad (6)$$

$$2NAD + UQH_2 \rightarrow 2NADH + UQ \quad (7)$$

$$NO_3^- (2NO_2^-) + UQH_2 \xrightarrow{NAR\ /\ NAP\ /\ NIR} NO_2^- (2NO) + UQ + H_2O \quad (8)$$

$$2NO\ (N_2O) + 2NADH^+ \xrightarrow{NOR\ /\ NorZ} N_2O\ (N_2) + 2NAD^+ + H_2O \quad (9)$$

Where H—R, organic carbon; UQ, ubiquinone (coenzyme Q); $UQH_2$, reduced UQ; DeH, dehydrogenase; NAD, nicotinamide adenine dinucleotide; NADH, reduced NAD. In reaction (6), the OC could be utilized as H—R to form $UQH_2$ and initiate reactions (7)-(9). An extra electron donor will be consumed when IC is dosed to form OC for reaction (6), resulting in weaker denitrification. Consequently, the addition of OC was suggested

as a strategy to enhance denitrification and control the emission of $NO_2^-$ and $N_2O$ in Fe(0)-ADN process, and an optimum dosages of 0.25 mmol C/mmol N was obtained.

### 3.5 Microorganisms related to $NO_2^-$ and $N_2O$ accumulations

The smooth rarefaction curves shown in Fig. S3 confirmed the high quality of PCR products for HTS [52]. HTS process obtained the alpha diversity estimators (*Shannon*, *Ace*, *Simpson* and *Chao*) with relatively high coverage of over 0.997 (Table S1), suggesting that sequencing results were sufficient for the microbial community characterization [53, 54]. Microbial community constituents at phylum and class levels and the hierarchical heat-map were presented in Fig. 7. Phyla Proteobacteria and Bacteroidetes were abundant in all the samples covering 52-87% and 4-12% of the sequences, respectively. Noteworthy, the abundance of Proteobacteria shifted to 84%, 76% and 87% in the BioFe(II), BioFe(0) and BioH samples, respectively, compared to the 52% of IAS (Fig. 7(a)). Fig. 7(b) suggested that the enrichment of Proteobacteria was attributed to the increase of the abundance of β-Proteobacteria, covering 68%, 62% and 64% of the sequences in BioFe(II), BioFe(0) and BioH, respectively. This trend agrees with previous investigations that most autotrophic denitrifying bacteria (ADBs) belong to the classes of β- or γ-Proteobacteria [10, 12, 55].

Hierarchical heat-map on genomic DNA according to 16S rRNA HTS was structured with R-code. According to Fig. 7(c), the dominant genera significantly changed in the Fe(II)-, Fe(0)- and H-ADN systems compared to IAS. PCA showed in Fig. 7(d) explained PC1 of 61% and PC2 of 18%, which also showed that BioFe(II), BioFe(0) and BioH were more closely clustered and far away from the IAS. Existing studies have verified the functional ADBs in H-ADN [31, 56], S-ADN [57], Fe(II)-ADN [47, 58] and Fe(0)-ADN [12]. However, their relationships with the $NO_2^-$ and $N_2O$ accumulation remained unexplored. As Fig. 7(c) shows, nine genera were confirmed as dominant (≥ 2%)

microbes, including 6 ADBs, i.e., *Thiobacillus*, *Thauera*, *Acidovorax*, *Ferritrotrophicum*, *Sulfurimonas* and *Denitratisoma*. Their relative abundances varied among the BioFe(II), BioFe(0) and BioH samples, indicating that ADBs compositions varied with the change of electron donor. Genus *Thiobacillus* dominated BioFe(II) (42%), followed by *Ferritrotrophicum* (5%). However, their abundances markedly decreased in BioH with a sharp increase of *Thauera* from 4% to 34%. This result correlates with the observation of Mao et al. (2013) that *Thauera* was dominant in the H-ADN system. Meanwhile, *Thiobacillus* (28%), *Thauera* (8%) and *Ferritrotrophicum* (12%) were all abundant in BioFe(0). Specifically, genera *BD1-7_clade*, *Dechloromonas* and *vadinBC27* were also enriched in the samples, but their pure cultures still have not been identified as ADBs.

PCC and ANOVA analyses were applied to identify the correlation of dominant ADBs to denitrification and accumulation of $NO_2^-$ and $N_2O$. As Fig. 8 shows, Genera *Thiobacillus* showed a significant ($p < 0.05$) high positive correlation (PCC > 0.7) to denitrification rate, indicating that the enrichment of *Thiobacillus* is beneficial for strengthening denitrification. Genera *Denitratisoma* was also positively correlated to the denitrification rate, but the correlation was not statistically significant ($p > 0.05$). *Thauera* and *Acidovorax* were found significantly negatively correlated to denitrification rate ($-0.7 < PCC < -0.4$, $p < 0.05$). As for the relationship of dominant ADBs to $NO_2^-$ and $N_2O$ accumulation, *Thiobacillus* exhibited a significant positive correlation to $NO_2^-$ accumulation (PCC = 0.64, $p = 0.02$) and a significantly high positive correlation to $N_2O$ emission (PCC = 0.82, $p = 0.03$). This result suggests that the enrichment of *Thiobacillus* could aggravate the high $NO_2^-$ and $N_2O$ accumulation. Comparatively, both *Thauera* and *Acidovorax* showed significant negative correlation ($-0.7 < PCC < -0.4$, $p < 0.05$) to $NO_2^-$ accumulation. Additionally, *Thauera* exhibited a significant high negative correlation (PCC = –0.87, $p = 0.02$) and exhibited *Acidovorax* significant negative

correlation (PCC = –0.67, $p = 0.01$) to $N_2O$ accumulation. Therefore, the genera *Thauera* and *Acidovorax* effectively reduced the accumulation of $NO_2^-$ and $N_2O$. Consequently, Fe(II)-ADN is effective in $NO_3^-$ reduction with the high abundance of *Thiobacillus*, whereas the presence of $H_2$ can increase the abundances of *Thauera* and *Acidovorax* which are effective in reducing $NO_2^-$ and $N_2O$ accumulation.

**3.6 Enzyme activities and gene quantities**

Activities of the key enzymes and quantities of the functional genes in Fe(II)-, Fe(0)- and H-ADN processes were explored to provide an in-depth understanding of their connections $NO_2^-$ and $N_2O$ accumulation. Fig. 9 showed a marked variation of enzyme activities and gene quantities with the different electron donor compositions. As Fig. 9(a) shows, NAP and NAR both existed in the samples, but NAR presented higher activities in all the BioFe(II), BioFe(0) and BioH samples. Moreover, the variation of NAR followed the change of the quantity of gene *napA*, indicating that *napA* mainly encoded NAR for $NO_3^-$ reduction. Comparatively, the activity of NAR in BioFe(0) and BioH were 2.4- and 1.9-fold higher than that in BioFe(II), demonstrating that the chemical $NO_3^-$ reduction by $Fe^{2+}$ has contributed to the $NO_3^-$ reduction in Fe(II)-ADN, which well confirmed the research of Margalef-Marti et al. (2020).

All the BioFe(II), BioFe(0) and BioH samples obtained high NIR activities, which were 3.8-, 4.5- and 4.3-folders higher than the IAS, respectively. Comparatively, the activity of NIR in sample BioFe(II) is the lowest among the three samples. As NIR has been confirmed as the main enzyme that catalyze the further reduction of $NO_2^-$ into NO [29], the reduction of its activity would decrease $NO_2^-$ consumption rate during denitrification and aggravate $NO_2^-$ accumulation. This result confirmed the trend of $NO_2^-$ accumulation in Fig. 2 that the Fe(II)-ADN systems obtained the highest accumulating percentage of 24.0%. In terms of the genes *nirK* and *nirS* encoding NIR (Fig. 9(b)),

BioFe(0) and BioH obtained significantly higher ($p < 0.05$) *nirK* abundances than BioFe(II), while both BioFe(0) and BioFe(II) have much higher *nirS* abundances than BioH. This result indicated that the presence of $H_2$ and Fe(II) in the ADN system could enhance the abundances of genes *nirK* and *nirS*, respectively. Additionally, both BioFe(0) and BioH have a much higher NosZ activity (5.3- and 7.7-fold, respectively) than the IAS, while that is only 1.1-fold in Fe(II)-ADN. This result strongly confirmed that the $N_2O$ accumulation of Fe(0)- and H-ADN processes were significantly lower ($p < 0.05$) than Fe(II)-ADN process (Fig. 2(d)). Meanwhile, the abundance of *nosZ* in sample BioFe(II) is significantly lower ($p < 0.05$) than that in samples BioFe(0) and BioH, which is the direct cause of low NosZ activity in BioFe(II) [59]. The observations of López et al. (2017) and Li et al. (2017) showed that NosZ could be enriched in H-ADN system, and the $N_2O$ reduction would not be inhibited even at a low $H_2$ concentration of 0.02 mg/L. Hence, it could be concluded from the results of this study that the presence of H-ADN could increase the abundances of genes *nirK* and *nosZ* in Fe(II)- and Fe(0)-ADN process with high NIR and NosZ activities, which could effectively control the accumulation of $NO_2^-$ and $N_2O$, respectively.

## 4 Conclusion

This study first systematically evaluated the accumulation of $N_2O$ and $NO_2^-$ in Fe(II)-ADN and Fe(0)-ADN processes along with the investigation of mechanisms, impact factors, and molecular biological characteristics. Fe(II)-ADN was more efficient in $NO_3^-$ reduction than Fe(0)-ADN, but less efficient in reducing $NO_2^-$ and $N_2O$. A much higher $NO_2^-$ and $N_2O$ accumulation was also found in Fe(II)-ADN. Fe(0)-ADN was a combined process of Fe(II)- and H-ADN by in-situ generating Fe(II) and $H_2$ from Fe(0). The presence of H-ADN significantly ($p < 0.05$) reduced $NO_2^-$/$N_2O$ accumulation. Fe(II)- and H-ADN mainly contributed to reducing $NO_3^-$ and $NO_2^-$/$N_2O$ in Fe(0)-ADN,

respectively. Optimum pH, temperature and OC dosage of 7.5, 30-35 °C and 0.25 mmol C/mmol N were respectively confirmed for Fe(0)-ADN for high denitrification rate and low $NO_2^-$/$N_2O$ accumulation. *Thiobacillus* was the main contributor to $NO_3^-$ reduction in the ADN processes, and *Thauera* and *Acidovorax* mainly contributed $NO_2^-$ and $N_2O$ reduction. NIR encoded by *nirK* and NosZ encoded by *nosZ* respectively catalyzed the further reduction of $NO_2^-$ and $N_2O$ into $N_2$. The results provided a comprehensive and in-depth understanding of $N_2O$/$NO_2^-$ accumulation in Fe(II)-/Fe(0)-ADN processes, which could contribute to the application of these processes with a controlled secondary pollutants emission. This work was performed through lab-scale batch tests, evaluations in continuous and upscaled systems are still required in future studies.

**Acknowledgments**

This research was financially supported by the National Natural Science Foundation of China [grant numbers 51778040, 51278034].

**References**

[1] A. Bhatnagar, M. Sillanpää, A review of emerging adsorbents for nitrate removal from water, Chemical Engineering Journal 168(2) (2011) 493-504. https://doi.org/10.1016/j.cej.2011.01.103.

[2] A. Wei, J. Ma, J. Chen, Y. Zhang, J. Song, X. Yu, Enhanced nitrate removal and high selectivity towards dinitrogen for groundwater remediation using biochar-supported nano zero-valent iron, Chemical Engineering Journal 353 (2018) 595-605. https://doi.org/10.1016/j.cej.2018.07.127.

[3] D. Liang, W. He, C. Li, F. Wang, J.C. Crittenden, Y. Feng, Remediation of nitrate contamination by membrane hydrogenotrophic denitrifying biofilm integrated in microbial electrolysis cell, Water Research 188 (2021) 116498-116498. https://doi.org/10.1016/j.watres.2020.116498.

[4] D. Liang, W. He, C. Li, F. Wang, J.C. Crittenden, Y. Feng, Remediation of nitrate contamination by membrane hydrogenotrophic denitrifying biofilm integrated in microbial electrolysis cell, Water Research 188 (2021) 116498. https://doi.org/https://doi.org/10.1016/j.watres.2020.116498.

[5] K.-C. Lee, B.E. Rittmann, Applying a novel autohydrogenotrophic hollow-fiber membrane biofilm reactor for denitrification of drinking water, Water Research 36(8) (2002) 2040-2052. https://doi.org/https://doi.org/10.1016/S0043-1354(01)00425-0.

[6] F. Di Capua, F. Pirozzi, P.N.L. Lens, G. Esposito, Electron donors for autotrophic

denitrification, Chemical Engineering Journal 362 (2019) 922-937. https://doi.org/10.1016/j.cej.2019.01.069.

[7] H. Liu, W. Zeng, Z. Fan, J. Li, M. Zhan, Y. Peng, Effect of iron on enhanced nitrogen removal from wastewater by sulfur autotrophic denitrification coupled to heterotrophic denitrification under different substrate ratios, Chemical Engineering Journal 421 (2021) 129828. https://doi.org/10.1016/j.cej.2021.129828.

[8] C. Zeng, Q. Su, L. Peng, L. Sun, Q. Zhao, X. Diao, H. Lu, Elemental sulfur-driven autotrophic denitrification for advanced nitrogen removal from mature landfill leachate after PN/A pretreatment, Chemical Engineering Journal 410 (2021) 128256. https://doi.org/10.1016/j.cej.2020.128256.

[9] Y.D. Scherson, G.F. Wells, S.-G. Woo, J. Lee, J. Park, B.J. Cantwell, C.S. Criddle, Nitrogen removal with energy recovery through N2O decomposition, Energy Environ. Sci 6(1) (2013) 241-248. https://doi.org/10.1039/C2EE22487A.

[10] K. Kiskira, S. Papirio, E.D. van Hullebusch, G. Esposito, Fe(II)-mediated autotrophic denitrification: A new bioprocess for iron bioprecipitation/biorecovery and simultaneous treatment of nitrate-containing wastewaters, International Biodeterioration & Biodegradation 119 (2017) 631-648. https://doi.org/https://doi.org/10.1016/j.ibiod.2016.09.020.

[11] P. Wang, C. Wang, Y. Xu, J. Hou, F. Zhang, Q. Zhou, G. You, Zero valent iron supported biological denitrification for farmland drainage treatments with low organic carbon: Performance and potential mechanisms, Science of the Total Environment 689 (2019) 1044-1053. https://doi.org/10.1016/j.scitotenv.2019.06.488.

[12] S. Deng, S. Peng, B. Xie, X. Yang, S. Sun, H. Yao, D. Li, Influence characteristics and mechanism of organic carbon on denitrification, N2O emission and NO2− accumulation in the iron [Fe(0)]-oxidizing supported autotrophic denitrification process, Chemical Engineering Journal 393 (2020) 124736. https://doi.org/10.1016/j.cej.2020.124736.

[13] H. Gu, S. Lang, G. Song, S. Zhang, M. Niu, W. Liu, L. Shen, Enhanced chemical looping hydrogen production based on biomass ash-promoted iron ore oxygen carrier, Chemical Engineering Journal 360 (2019) 260-270. https://doi.org/10.1016/j.cej.2018.11.226.

[14] G. Zhen, X. Lu, Y.-Y. Li, Y. Liu, Y. Zhao, Influence of zero valent scrap iron (ZVSI) supply on methane production from waste activated sludge, Chemical Engineering Journal 263 (2015) 461-470. https://doi.org/10.1016/j.cej.2014.11.003.

[15] A.S. Oberoi, H. Huang, S.K. Khanal, L. Sun, H. Lu, Electron distribution in sulfur-driven autotrophic denitrification under different electron donor and acceptor feeding schemes, Chemical Engineering Journal 404 (2021) 126486. https://doi.org/10.1016/j.cej.2020.126486.

[16] B.A. Till, L.J. Weathers, P.J.J. Alvarez, Fe(0)-Supported Autotrophic Denitrification, Environmental Science & Technology 32(5) (1998) 634-639. https://doi.org/10.1021/es9707769.

[17] M.J. Kampschreur, H. Temmink, R. Kleerebezem, M.S.M. Jetten, M.C.M. van

Loosdrecht, Nitrous oxide emission during wastewater treatment, Water Research 43(17) (2009) 4093-4103. https://doi.org/10.1016/j.watres.2009.03.001.

[18] L. Zhang, C. Zhang, C. Hu, H. Liu, Y. Bai, J. Qu, Sulfur-based mixotrophic denitrification corresponding to different electron donors and microbial profiling in anoxic fluidized-bed membrane bioreactors, Water Research 85 (2015) 422-431. https://doi.org/10.1016/j.watres.2015.08.055.

[19] A. Rodriguez-Caballero, I. Aymerich, R. Marques, M. Poch, M. Pijuan, Minimizing N2O emissions and carbon footprint on a full-scale activated sludge sequencing batch reactor, Water Research 71 (2015) 1-10. https://doi.org/https://doi.org/10.1016/j.watres.2014.12.032.

[20] I.S. Thakur, K. Medhi, Nitrification and denitrification processes for mitigation of nitrous oxide from waste water treatment plants for biovalorization: Challenges and opportunities, Bioresource Technology 282 (2019) 502-513. https://doi.org/10.1016/j.biortech.2019.03.069.

[21] Y. Wang, X. Lin, D. Zhou, L. Ye, H. Han, C. Song, Nitric oxide and nitrous oxide emissions from a full-scale activated sludge anaerobic/anoxic/oxic process, Chemical Engineering Journal 289 (2016) 330-340. https://doi.org/10.1016/j.cej.2015.12.074.

[22] L. Zhang, C. Zhang, C. Hu, H. Liu, J. Qu, Denitrification of groundwater using a sulfur-oxidizing autotrophic denitrifying anaerobic fluidized-bed MBR: performance and bacterial community structure, Applied Microbiology and Biotechnology 99(6) (2014) 2815-2827. https://doi.org/10.1007/s00253-014-6113-9.

[23] M.R. Awual, A.M. Asiri, M.M. Rahman, N.H. Alharthi, Assessment of enhanced nitrite removal and monitoring using ligand modified stable conjugate materials, Chemical Engineering Journal 363 (2019) 64-72. https://doi.org/10.1016/j.cej.2019.01.125.

[24] Y. Zhou, A. Oehmen, M. Lim, V. Vadivelu, W.J. Ng, The role of nitrite and free nitrous acid (FNA) in wastewater treatment plants, Water Research 45(15) (2011) 4672-4682. https://doi.org/https://doi.org/10.1016/j.watres.2011.06.025.

[25] V. Rocher, A.M. Laverman, J. Gasperi, S. Azimi, S. Guérin, S. Mottelet, T. Villières, A. Pauss, Nitrite accumulation during denitrification depends on the carbon quality and quantity in wastewater treatment with biofilters, Environmental Science and Pollution Research 22(13) (2015) 10179-10188. https://doi.org/10.1007/s11356-015-4196-1.

[26] Y. Zhou, M. Pijuan, R.J. Zeng, Z. Yuan, Free Nitrous Acid Inhibition on Nitrous Oxide Reduction by a Denitrifying-Enhanced Biological Phosphorus Removal Sludge, Environmental Science & Technology 42(22) (2008) 8260-8265. https://doi.org/10.1021/es800650j.

[27] Y. Liu, L. Peng, H.H. Ngo, W. Guo, D. Wang, Y. Pan, J. Sun, B.-J. Ni, Evaluation of Nitrous Oxide Emission from Sulfide- and Sulfur-Based Autotrophic Denitrification Processes, Environmental Science & Technology 50(17) (2016) 9407-9415. https://doi.org/10.1021/acs.est.6b02202.

[28] S. Deng, D. Li, X. Yang, Q. Cai, S. Peng, X. Peng, H. Yao, B. Xie, Novel

characteristics on micro-electrolysis mediated Fe(0)-oxidizing autotrophic denitrification with aeration: Efficiency, iron-compounds transformation, N2O and NO2− accumulation, and microbial characteristics, Chemical Engineering Journal (2019) 123409. https://doi.org/10.1016/j.cej.2019.123409.

[29] H. Chen, X. Zhao, Y. Cheng, M. Jiang, X. Li, G. Xue, Iron Robustly Stimulates Simultaneous Nitrification and Denitrification Under Aerobic Conditions, Environmental Science & Technology 52(3) (2018) 1404-1412. https://doi.org/10.1021/acs.est.7b04751.

[30] J.C. López, E. Porca, G. Collins, R. Pérez, A. Rodríguez-Alija, R. Muñoz, G. Quijano, Biogas-based denitrification in a biotrickling filter: Influence of nitrate concentration and hydrogen sulfide, Biotechnology and Bioengineering 114(3) (2017) 665-673. https://doi.org/10.1002/bit.26092.

[31] P. Li, Y. Wang, J. Zuo, R. Wang, J. Zhao, Y. Du, Nitrogen Removal and N2O Accumulation during Hydrogenotrophic Denitrification: Influence of Environmental Factors and Microbial Community Characteristics, Environmental Science & Technology 51(2) (2017) 870-879. https://doi.org/10.1021/acs.est.6b00071.

[32] W. Yang, Q. Zhao, H. Lu, Z. Ding, L. Meng, G.-H. Chen, Sulfide-driven autotrophic denitrification significantly reduces N2O emissions, Water Research 90 (2016) 176-184. https://doi.org/10.1016/j.watres.2015.12.032.

[33] R. Margalef-Marti, R. Carrey, J.A. Benito, V. Marti, A. Soler, N. Otero, Nitrate and nitrite reduction by ferrous iron minerals in polluted groundwater: Isotopic characterization of batch experiments, Chemical Geology 548 (2020) 119691. https://doi.org/10.1016/j.chemgeo.2020.119691.

[34] W. Yang, Q. Zhao, H. Lu, Z. Ding, L. Meng, G.-H. Chen, Sulfide-driven autotrophic denitrification significantly reduces N2O emissions, Water Research 90 (2016) 176-184. https://doi.org/10.1016/j.watres.2015.12.032.

[35] D. Liang, W. He, C. Li, Y. Yu, Z. Zhang, N. Ren, Y. Feng, Bidirectional electron transfer biofilm assisted complete bioelectrochemical denitrification process, Chemical Engineering Journal 375 (2019) 121960. https://doi.org/10.1016/j.cej.2019.121960.

[36] M. Zhang, G. Zhangzhu, S. Wen, H. Lu, R. Wang, W. Li, S. Ding, A. Ghulam, P. Zheng, Chemolithotrophic denitrification by nitrate-dependent anaerobic iron oxidizing (NAIO) process: Insights into the evaluation of seeding sludge, Chemical Engineering Journal 345 (2018) 345-352. https://doi.org/10.1016/j.cej.2018.03.156.

[37] S. Biswas, P. Bose, Zero-Valent Iron-Assisted Autotrophic Denitrification, Journal of Environmental Engineering 131(8) (2005) 1212-1220. https://doi.org/10.1061/(ASCE)0733-9372(2005)131:8(1212).

[38] S. Deng, B. Xie, Q. Kong, S. Peng, H. Wang, Z. Hu, D. Li, An oxic/anoxic-integrated and Fe/C micro-electrolysis-mediated vertical constructed wetland for decentralized low-carbon greywater treatment, Bioresource Technology (2020) 123802. https://doi.org/https://doi.org/10.1016/j.biortech.2020.123802.

[39] S. Deng, Q. Wang, Q. Cai, S.L. Ong, J. Hu, Efficient bio-refractory industrial

wastewater treatment with mitigated membrane fouling in a membrane bioreactor strengthened by the micro-scale ZVI@GAC galvanic-cells-initiated radical generation and coagulation processes, Water Research 209 (2021) 117943. https://doi.org/10.1016/j.watres.2021.117943.

[40] L.A. Robertson, J.G. Kuenen, Aerobic denitrification: a controversy revived, Archives of microbiology 139(4) (1984) 351-354. https://doi.org/10.1007/bf00408378.

[41] E. Sahinkaya, N. Dursun, A. Kilic, S. Demirel, S. Uyanik, O. Cinar, Simultaneous heterotrophic and sulfur-oxidizing autotrophic denitrification process for drinking water treatment: Control of sulfate production, Water Research 45(20) (2011) 6661-6667. https://doi.org/10.1016/j.watres.2011.09.056.

[42] J.R. Rumble, D.R. Lide, T.J. Bruno, CRC handbook of chemistry and physics: a ready-reference book of chemical and physical data, 2017-2018, 98th ed., CRC Press, Boca Raton, 2017.

[43] G.F. Versteeg, W.P.M. Van Swaaij, Solubility and diffusivity of acid gases (carbon dioxide, nitrous oxide) in aqueous alkanolamine solutions, Journal of Chemical and Engineering Data 33(1) (1988) 29-34. https://doi.org/10.1021/je00051a011.

[44] V. Matěj, S. iinská, J. Krejí, T. Janoch, Biological water denitrification—A review, Enzyme and Microbial Technology 14(3) (1992) 170–183.

[45] H. Liu, Z. Chen, Y. Guan, S. Xu, Role and application of iron in water treatment for nitrogen removal: A review, Chemosphere 204 (2018) 51-62. https://doi.org/10.1016/j.chemosphere.2018.04.019.

[46] Y. Pan, L. Ye, B.-J. Ni, Z. Yuan, Effect of pH on N2O reduction and accumulation during denitrification by methanol utilizing denitrifiers, Water Research 46(15) (2012) 4832-4840. https://doi.org/10.1016/j.watres.2012.06.003.

[47] M. Chen, X. Zhou, X. Chen, Q. Cai, R.J. Zeng, S. Zhou, Mechanisms of nitrous oxide emission during photoelectrotrophic denitrification by self-photosensitized Thiobacillus denitrificans, Water Research 172 (2020) 115501-115501. https://doi.org/10.1016/j.watres.2020.115501.

[48] D. Martin, J.M. Salminen, R.M. Niemi, I.M. Heiskanen, M.J. Valve, P.P. Hellstén, T.H. Nystén, Acetate and ethanol as potential enhancers of low temperature denitrification in soil contaminated by fur farms: A pilot-scale study, Journal of Hazardous Materials 163(2) (2009) 1230-1238. https://doi.org/10.1016/j.jhazmat.2008.07.092.

[49] M. Kurt, I.J. Dunn, J.R. Bourne, Biological denitrification of drinking water using autotrophic organisms with H2 in a fluidized-bed biofilm reactor, Biotechnology and Bioengineering 29(4) (1987) 493-501. https://doi.org/10.1002/bit.260290414.

[50] L.S. Poh, X. Jiang, Z. Zhang, Y. Liu, W.J. Ng, Y. Zhou, N2O accumulation from denitrification under different temperatures, Applied Microbiology and Biotechnology 99(21) (2015) 9215-9226. https://doi.org/10.1007/s00253-015-6742-7.

[51] Q. He, Q. Song, S. Zhang, W. Zhang, H. Wang, Simultaneous nitrification,

denitrification and phosphorus removal in an aerobic granular sequencing batch reactor with mixed carbon sources: reactor performance, extracellular polymeric substances and microbial successions, Chemical Engineering Journal 331 (2018) 841-849. https://doi.org/10.1016/j.cej.2017.09.060.

[52] W. Gong, B. Xie, S. Deng, Y. Fan, X. Tang, H. Liang, Enhancement of anaerobic digestion effluent treatment by microalgae immobilization: Characterized by fluorescence excitation-emission matrix coupled with parallel factor analysis in the photobioreactor, Science of the Total Environment 678 (2019) 105-113. https://doi.org/10.1016/j.scitotenv.2019.04.440.

[53] S. Peng, S. Deng, D. Li, B. Xie, X. Yang, C. Lai, S. Sun, H. Yao, Iron-carbon galvanic cells strengthened anaerobic/anoxic/oxic process (Fe/C-A2O) for high-nitrogen/phosphorus and low-carbon sewage treatment, Science of the Total Environment 722 (2020) 137657. https://doi.org/10.1016/j.scitotenv.2020.137657.

[54] H. Pang, Y. Chen, J. He, D. Guo, X. Pan, Y. Ma, F. Qu, J. Nan, Cation exchange resin-induced hydrolysis for improving biodegradability of waste activated sludge: Characterization of dissolved organic matters and microbial community, Bioresource Technology 302 (2020) 122870-122870. https://doi.org/10.1016/j.biortech.2020.122870.

[55] A. Mohseni-Bandpi, D.J. Elliott, M.A. Zazouli, Biological nitrate removal processes from drinking water supply-a review, Journal of Environmental Health Science & Engineering 11(1) (2013) 35-35. https://doi.org/10.1186/2052-336X-11-35.

[56] Y. Mao, Y. Xia, T. Zhang, Characterization of Thauera-dominated hydrogen-oxidizing autotrophic denitrifying microbial communities by using high-throughput sequencing, Bioresource Technology 128 (2013) 703-710. https://doi.org/10.1016/j.biortech.2012.10.106.

[57] G. Wu, Z. Li, Y. Huang, F. Zan, J. Dai, J. Yao, B. Yang, G. Chen, L. Lei, Electrochemically assisted sulfate reduction autotrophic denitrification nitrification integrated (e-SANI®) process for high-strength ammonium industrial wastewater treatment, Chemical Engineering Journal 381 (2020) 122707. https://doi.org/10.1016/j.cej.2019.122707.

[58] X. Luo, J. Su, P. Shao, H. Liu, X. Luo, Efficient autotrophic denitrification performance through integrating the bio-oxidation of Fe(II) and Mn(II), Chemical Rngineering Journal 348 (2018) 669-677. https://doi.org/10.1016/j.cej.2018.05.021.

[59] J. Harter, M. El-Hadidi, D.H. Huson, A. Kappler, S. Behrens, Soil biochar amendment affects the diversity of nosZ transcripts: Implications for N2O formation, Scientific Reports 7(1) (2017) 1-14. https://doi.org/10.1038/s41598-017-03282-y.

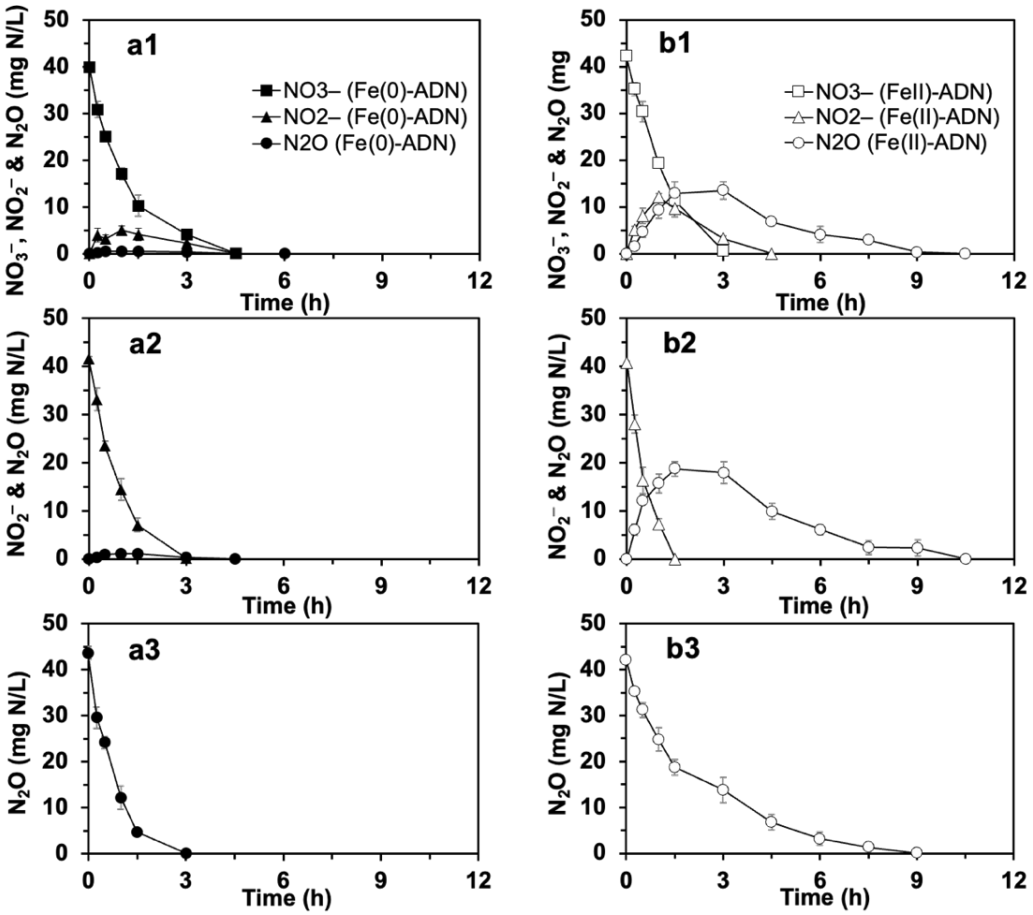


Fig. 1. Denitrifying characteristics of Fe(0)-ADN (a1, a2 and a3) and Fe(II)-ADN (b1, b2 and b3) when using $NO_3^-$ (a1 and b1), $NO_2^-$ (a2 and b2), and $N_2O$ (a3 and b3) as sole electron acceptor.

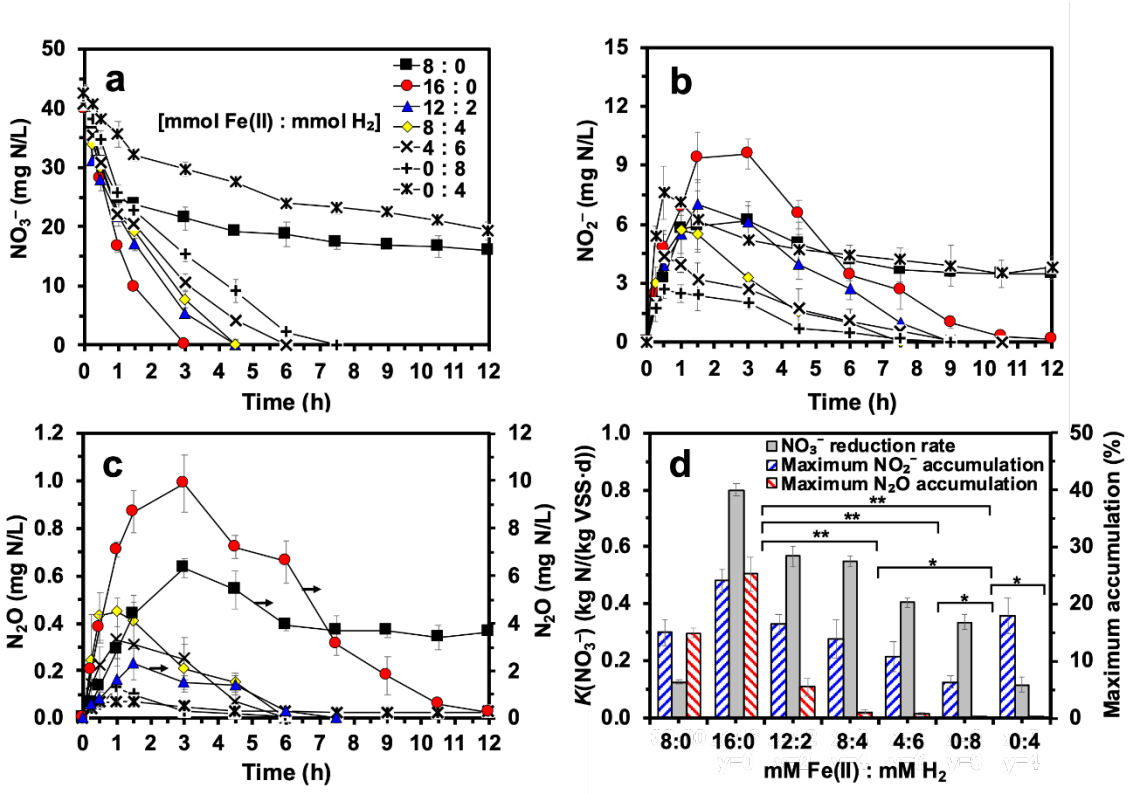


Fig. 2. The roles of Fe(II)-ADN and H-ADN in denitrification and $NO_2^-$/$N_2O$ accumulation. a, $NO_3^-$ reduction; b, $NO_2^-$ accumulation; c, $N_2O$ accumulation; and d, specific $NO_3^-$ reduction rate ($K(NO_3^-)$) and the maximum $NO_2^-$/$N_2O$ accumulation percentages. *, statistically insignificant ($p > 0.05$); **, statistically significant ($p < 0.05$). Error bars represent the standard deviation (n = 3).

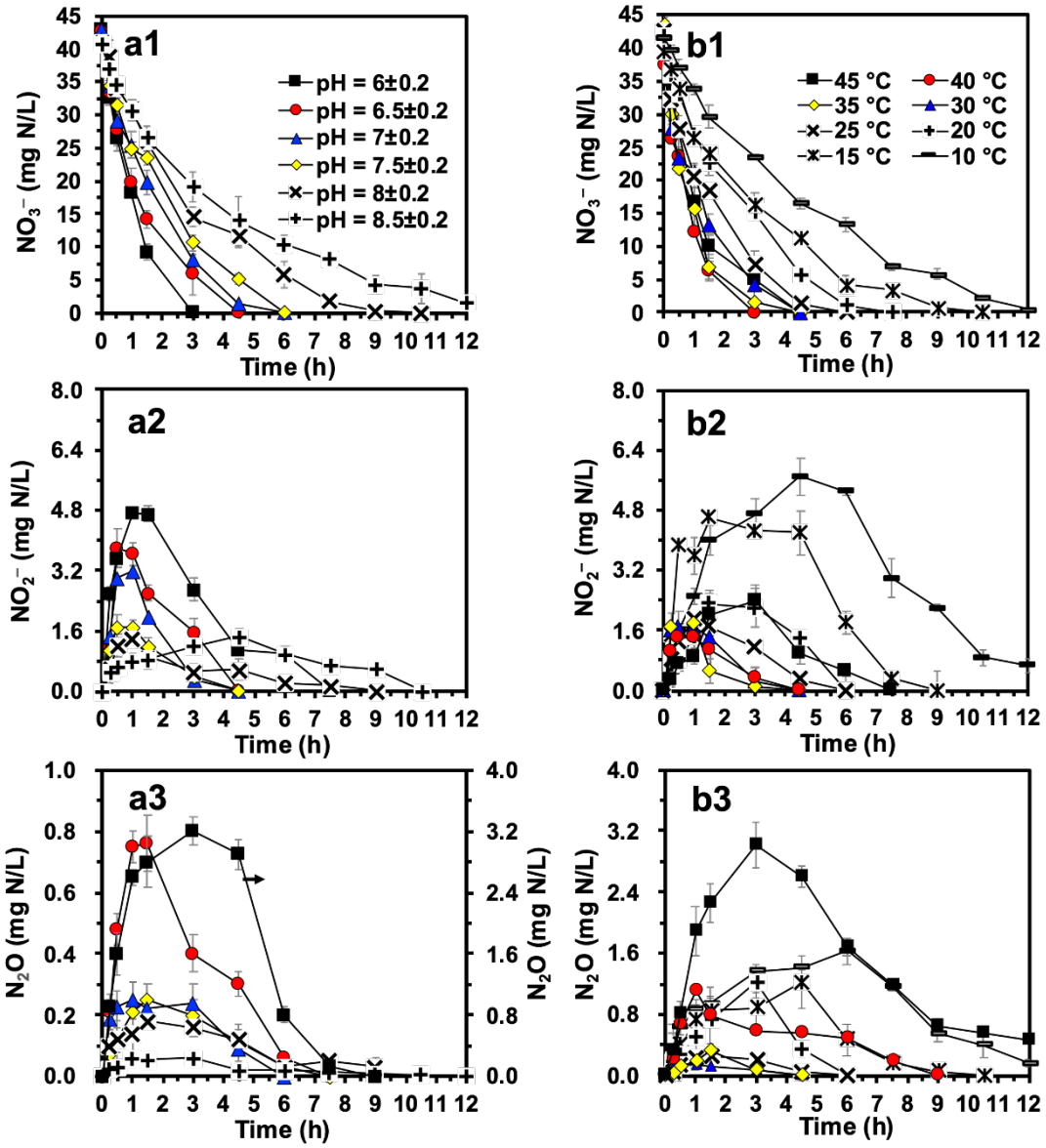


Fig. 3. Influence of (a1, a2 and a3) pH and (b1, b2 and b3) temperature on the $NO_2^-$ /$N_2O$ accumulation of Fe(0)-ADN: a1 and b1, $NO_3^-$ reduction; a2 and b2, $NO_2^-$ accumulation; a3 and b3, $N_2O$ accumulation. Error bars represent the standard deviation (n = 3).

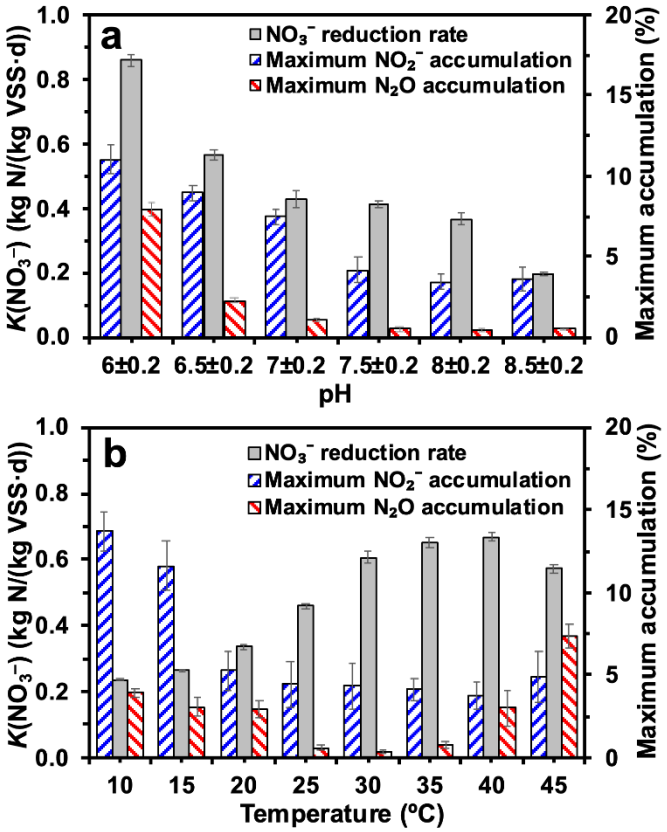


Fig. 4. Influence of (a) pH and (b) temperature on specific $NO_3^-$ reduction rate ($K(NO_3^-)$) and the maximum $NO_2^-/N_2O$ accumulation percentage of Fe(0)-ADN. Error bars represent the standard deviation (n = 3).

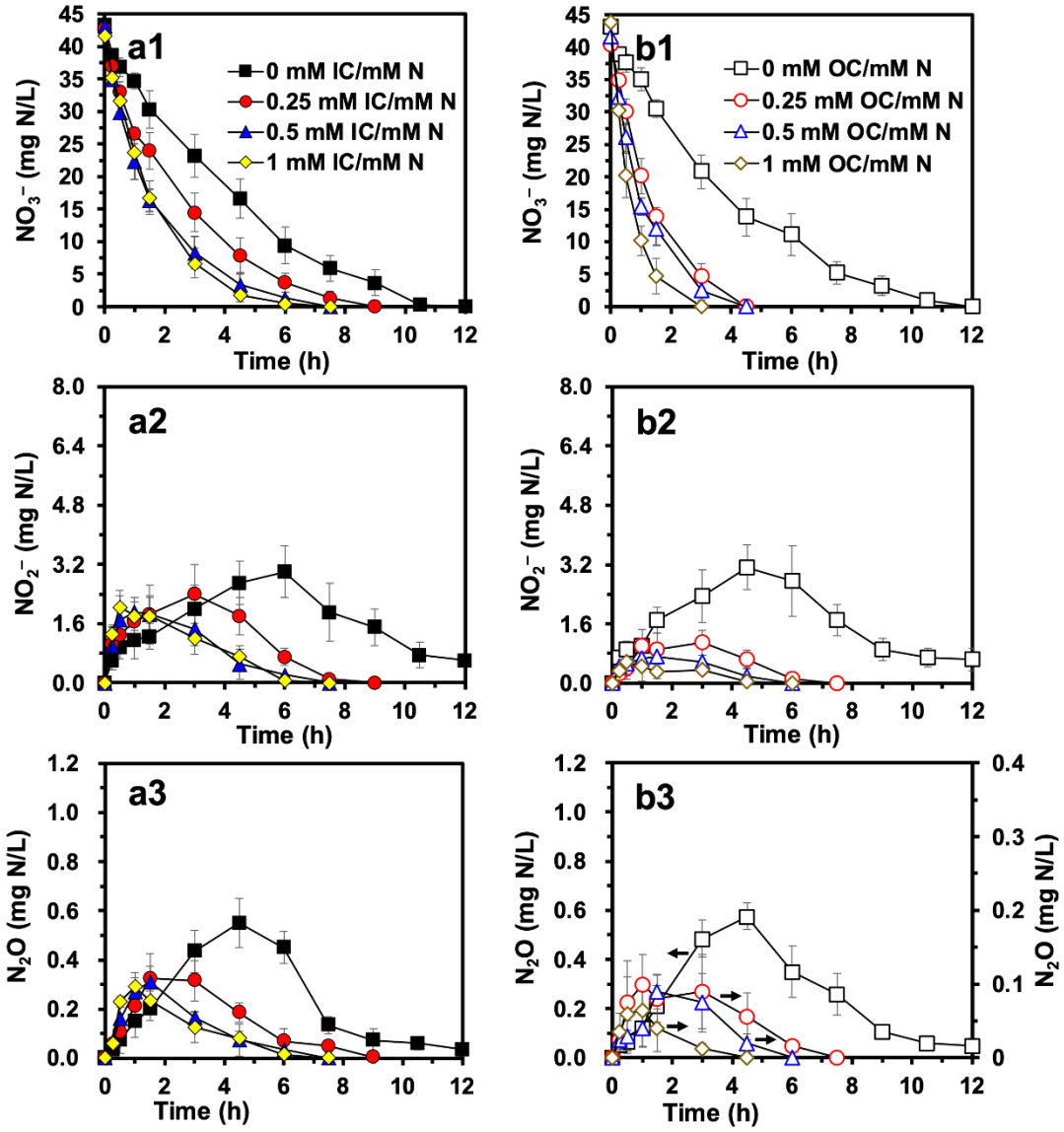


Fig. 5. $NO_2^-$ accumulation and $N_2O$ emission in Fe(0)-ADN under different (a1, a2 and a3) IC and (b1, b2 and b3) OC dosages: a1 and b1, variation of $NO_3^-$ concentration; a2 and b2, $NO_2^-$ accumulation; a3 and b3, $N_2O$ emission. Error bars represent the standard deviation (n = 3).

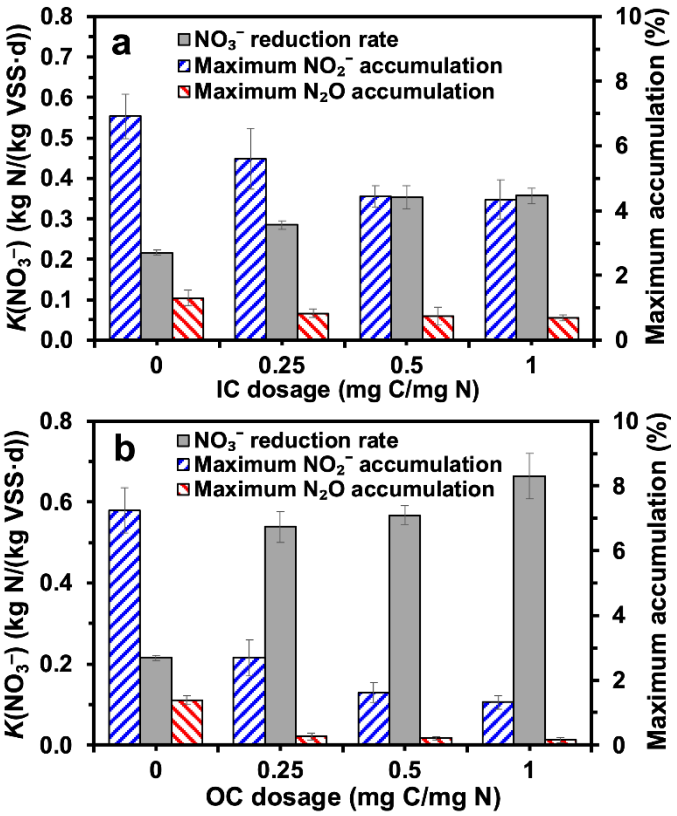


Fig. 6. Specific $NO_3^-$ reduction rate ($K(NO_3^-)$) and the maximum $NO_2^-/N_2O$ accumulation percentage under different (a) IC and (b) OC dosages. Error bars represent the standard deviation (n = 3).

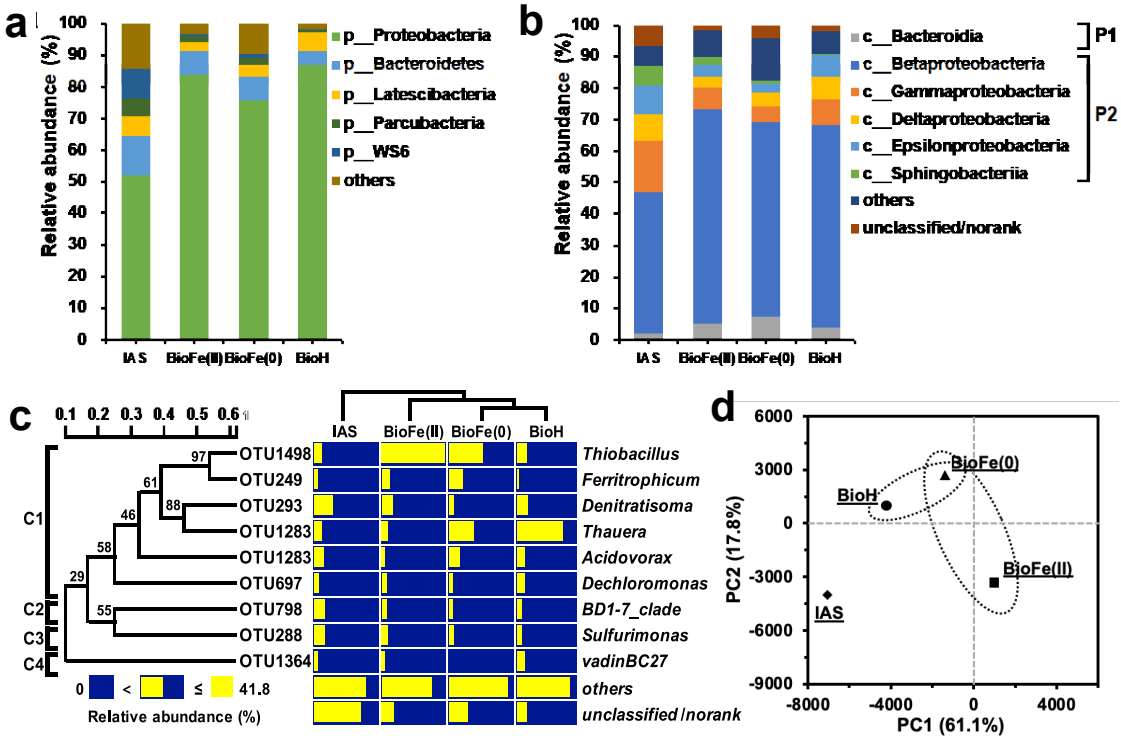


Fig. 7. Distribution of microbial communities into bacterial (a) phylum & (b) class, (c) the hierarchical heat map on genomic DNA according to the 16S rRNA HTS (Length of the yellow bar indicates the relative abundance, which is in the range of 0-41.8%.), and (d) the result of PCA. Communities covering over 2% of the total sequences are presented. P1-P2 represent the phyla Proteobacteria and Bacteroidetes, respectively. C1-C4 represent the classes Betaproteobacteria, Gammaproteobacteria, Epsilonproteobacteria and Bacteroidia, respectively.

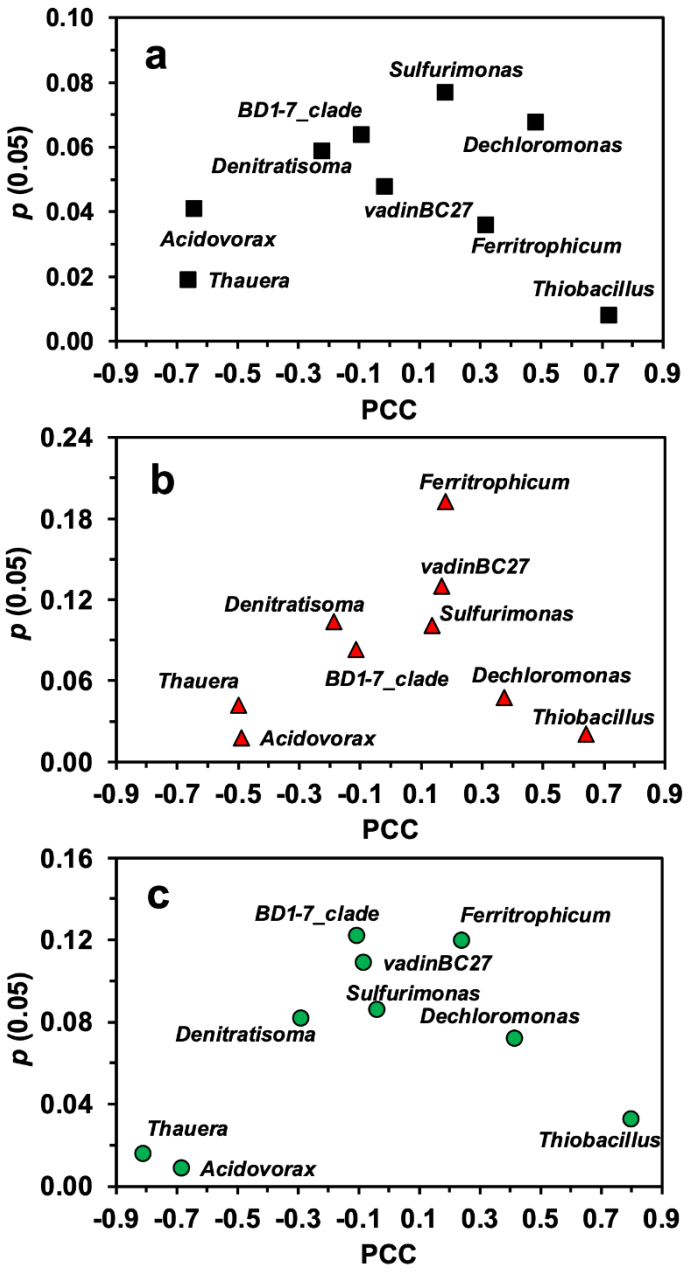


Fig. 8. PCC and ANOVA analysis on the correlations of bacteria to (a) denitrification, (b) $NO_2^-$ accumulation and (c) $N_2O$ accumulation. $1 \geq |PCC| > 0.7$, highly correlated; $0.7 \geq |PCC| \geq 0.4$, correlated; and $0 \leq |PCC| < 0.4$, uncorrelated. $p > 0.05$, statistically insignificant; $p < 0.05$, statistically significant.

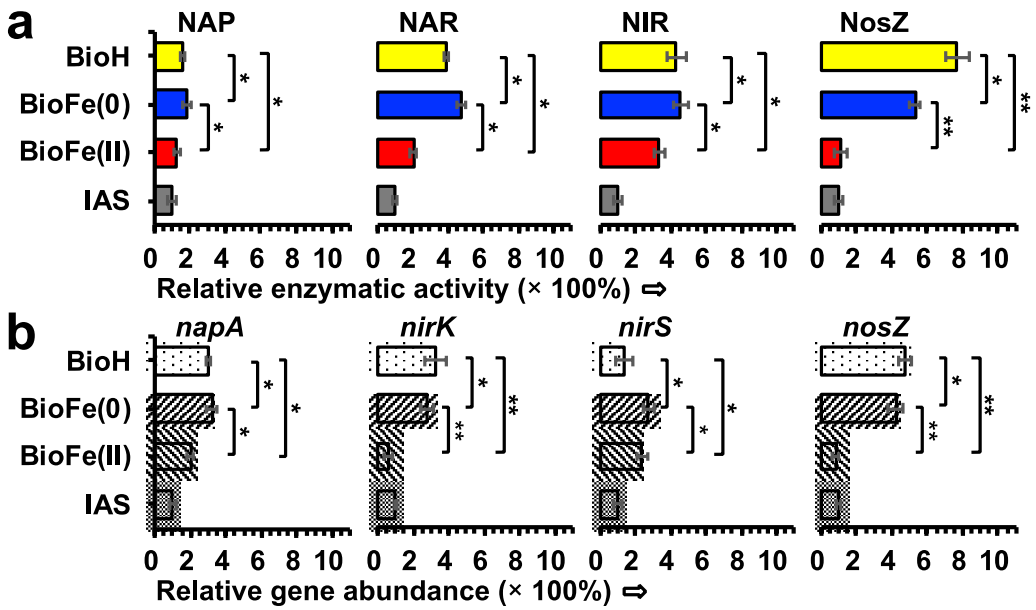


Fig. 9. Variation of (a) the activities of key denitrifying enzymes and (b) the quantities of functional denitrifying genes in Fe(II)-, Fe(0)- and H-ADN processes with the change of electron donor composition. *, statistically insignificant ($p > 0.05$); **, statistically significant ($p < 0.05$). Error bars represent the standard deviation (n = 3).

Table 1. The experimental groups and operation parameters.

| Experimental operations | | Sole electron acceptor | | | Electron donor | | | pH | Temperature (°C) | Carbon source | |
|---|---|---|---|---|---|---|---|---|---|---|---|
| | | $NO_3^-$ (mg N/L) | $NO_2^-$ (mg N/L) | $N_2O$ (mg N/L) | Fe(II) (mol/mol N) | Fe(0) (g Fe/mL) | $H_2$ (mmol/mmol N) | | | IC [b] (mmol C/mmol N) | OC [c] (mmol C/mmol N) |
| Group A: Characterize the reduction of $NO_3^-$, $NO_2^-$ and $N_2O$ in Fe(II)- and Fe(0)-ADN [a] | I | 40 | 0 | 0 | 7.6 | 0 | 0 | 7 ± 0.2 | 25 ± 1 | 1 | 0 |
| | II | 0 | 40 | 0 | 7.6 | 0 | 0 | 7 ± 0.2 | 25 ± 1 | 1 | 0 |
| | III | 0 | 0 | 40 | 7.6 | 0 | 0 | 7 ± 0.2 | 25 ± 1 | 1 | 0 |
| | IV | 40 | 0 | 0 | 0 | 0.4 | 0 | 7 ± 0.2 | 25 ± 1 | 1 | 0 |
| | V | 0 | 40 | 0 | 0 | 0.4 | 0 | 7 ± 0.2 | 25 ± 1 | 1 | 0 |
| | VI | 0 | 0 | 40 | 0 | 0.4 | 0 | 7 ± 0.2 | 25 ± 1 | 1 | 0 |
| Group B: Investigate the contributions of Fe(II) and $H_2$ on $NO_2^-$ and $N_2O$ accumulation | I | 40 | 0 | 0 | 8 | 0 | 0 | 7 ± 0.2 | 25 ± 1 | 1 | 0 |
| | II | 40 | 0 | 0 | 16 | 0 | 0 | 7 ± 0.2 | 25 ± 1 | 1 | 0 |
| | III | 40 | 0 | 0 | 12 | 0 | 2 | 7 ± 0.2 | 25 ± 1 | 1 | 0 |
| | IV | 40 | 0 | 0 | 8 | 0 | 4 | 7 ± 0.2 | 25 ± 1 | 1 | 0 |
| | V | 40 | 0 | 0 | 4 | 0 | 6 | 7 ± 0.2 | 25 ± 1 | 1 | 0 |
| | VI | 40 | 0 | 0 | 0 | 0 | 8 | 7 ± 0.2 | 25 ± 1 | 1 | 0 |
| | VII | 40 | 0 | 0 | 0 | 0 | 4 | 7 ± 0.2 | 25 ± 1 | 1 | 0 |
| Group C: Factors affecting on | I | 40 | 0 | 0 | 0 | 0.4 | 0 | (6, 6.5, 7, 7.5, 8 and 8.5) ± 0.2 | 25 ± 1 | 1 | 0 |

| | | | | | | | | | | | |
|---|---|---|---|---|---|---|---|---|---|---|---|
| $N_2O$ and $NO_2^-$ accumulation | II | 40 | 0 | 0 | 0 | 0.4 | 0 | 7 ± 0.2 | (10, 15, 20, 25, 30, 35, 40 and 45) ± 1 | 0 | |
| | III | 40 | 0 | 0 | 0 | 0.4 | 0 | 7 ± 0.2 | 25 ± 1 | 0, 0.25, 0.5 and 1 | 0 |
| | IV | 40 | 0 | 0 | 0 | 0.4 | 0 | 7 ± 0.2 | 25 ± 1 | 0 | 0, 0.25, 0.5 and 1 |

[a] ADN, autotrophic denitrification; [b] IC, inorganic carbon; [c] OC, organic carbon.

**Table 2.** Kinetic analysis on Fe(0)- and Fe(II)-ADN processes for the reductive reactions of $NO_3^-$, $NO_2^-$ and $N_2O$.

| Processes | Electron accepters | Pseudo-first-order kinetics ($\ln C_t - \ln C_0 = -k_1 t$) | | | Pseudo-zero-order kinetics ($C_t - C_0 = -k_2 t$) | | |
|---|---|---|---|---|---|---|---|
| | | $k_1$ ($h^{-1}$) | $R^2$ | RSSQ | $k_2$ (mg $L^{-1}$ $h^{-1}$) | $R^2$ | RSSQ |
| Fe(0)-ADN | $NO_3^-$ | 1.2 | 0.91 | 60.6 | 11.1 | 0.57 | 540.8 |
| | $NO_2^-$ | 1.8 | 0.95 | 164.6 | 18.1 | 0.53 | 400.4 |
| | $N_2O$ | 1.9 | 0.96 | 96.2 | 20.2 | 0.65 | 666.2 |
| Fe(II)-ADN | $NO_3^-$ | 1.7 | 0.85 | 409.0 | 15.9 | 0.92 | 161.5 |
| | $NO_2^-$ | 3.8 | 0.76 | 294.8 | 29.9 | 0.90 | 149.0 |
| | $N_2O$ | 0.5 | 0.91 | 34.4 | 5.9 | 0.63 | 769.0 |